SURFACE TENSION EFFECTS ON BREAKING WAVES

E.F. Campana and **A. Iafrati**, INSEAN (Italian Ship Model Basin), Italy, E-mail: e.campana@insean.it

SUMMARY
The role played by surface tension onto the wave breaking flow generated by a submerged hydrofoil is numerically investigated by a two-fluids Navier-Stokes approach. Both the initial breaking establishment and the successive evolution are addressed. Increasing surface tension is found to progressively suppress the initial jet formation and the entrainment of air.

1. INTRODUCTION

The role played by surface tension on the initial transient and the successive evolution of the breaking wavy flow that takes place when a submerged hydrofoil moves beneath the free surface is numerically investigated.

The motivation for this activity stems from the need of understanding the breaking occurring at the ship bow at full scale. In model testing of ships with pronounced flare, the occurrence of breaking and the wave pattern downstream the impact point are affected by the strong action of surface tension and may significantly differ from the full scale one.

The study is carried out by using a two-fluids Navier-Stokes solver coupled with the Level-set technique for the interface capturing. To reduce the computational effort, an unsteady heterogeneous domain decomposition approach is employed, which uses a potential model to describe the flow about the hydrofoil and a viscous model to describe the flow in the free surface region. As suggested by Brackbill *et al.* [1] a continuum model is adopted to include surface tension effects in the momentum equation.

The numerical model has been deeply validated in the past and some results were presented at the last Workshop [2] while a more detailed description may be found in [3], along with some results concerning the shear flow developing just beneath the free surface as a consequence of the breaking establishment.

In the present work, three different flow regimes in the breaking zone are obtained by varying the surface tension coefficient. The flow about a NACA 0012 hydrofoil, 5 degrees angle of attack, is simulated in the same conditions as the original experiment by Duncan [4] but for the Reynolds number. Then the surface tension coefficient is increased in such a way the Weber number is halved twice. It is observed that the growing surface tension effect leads to different mechanisms in the wave breaking process with differences arising both in the initial transient and in the final quasi-steady stage.

2. DOMAIN DECOMPOSITION APPROACH

The flow about a submerged hydrofoil is numerically simulated with the help of a heterogeneous domain decomposition approach which uses a potential model to describe the flow about the hydrofoil vicinities and a viscous flow model to describe the flow in the free surface region. To allow the description of complex free surface configurations, a two-fluids model is used in conjunction with the Navier-Stokes equations. In the following, the numerical models employed in the two regions are briefly discussed along with the coupling procedure.

2.1 TWO-FLUIDS MODEL

The flow of air and water is approximated as that of a single incompressible fluid whose density and viscosity change across the interface. In an Eulerian frame of reference, local fluid properties changes with time only due to the interface motion. The dimensionless unsteady Navier-Stokes equations in generalized coordinates ξ_m are:

$$\frac{\partial U_m}{\partial \xi_m} = 0 \tag{1}$$

$$\begin{aligned}\frac{\partial}{\partial t}(J^{-1}u_i) + \frac{\partial}{\partial \xi_m}(U_m u_i) = &-\frac{1}{\varrho}\frac{\partial}{\partial \xi_m}\left(J^{-1}\frac{\partial \xi_m}{\partial x_i}p\right) \\ -J^{-1}\frac{\delta_{i2}}{Fr^2} &- \frac{\kappa}{\varrho\, We^2}\frac{\partial}{\partial \xi_m}\left(J^{-1}\frac{\partial \xi_m}{\partial x_i}H(d)\right) \\ &+\frac{1}{Re\,\varrho}\frac{\partial}{\partial \xi_m}\left(\mu G^{ml}\frac{\partial u_i}{\partial \xi_l} + \mu B^{mlji}\frac{\partial u_j}{\partial \xi_l}\right)\end{aligned} \tag{2}$$

where u_i is the $i-$th cartesian velocity component and the quantity

$$U_m = J^{-1}\frac{\partial \xi_m}{\partial x_j}u_j \tag{3}$$

is the volume flux through the ξ_m iso-surface where J^{-1} is the inverse of the Jacobian. In eq. (2)

$$Fr = \frac{U_r}{\sqrt{gL_r}}\ ,\ Re = \frac{U_r L_r \varrho_w}{\mu_w}\ ,\ We = U_r\sqrt{\frac{\varrho_w L_r}{\sigma}}$$

are the Froude, Reynolds and Weber numbers, respectively, with U_r,L_r denoting reference values for velocity and length. σ is the surface tension coefficient while ϱ_w, μ_w are the values of density and dynamic viscosity in water and are used as reference values. In equation (2)

$$G^{ml} = J^{-1}\frac{\partial \xi_m}{\partial x_j}\frac{\partial \xi_l}{\partial x_j}\ ,\ B^{mlji} = J^{-1}\frac{\partial \xi_m}{\partial x_j}\frac{\partial \xi_l}{\partial x_i}$$

are metric terms, κ is the local curvature and $H(d)$ is the Heaviside function based on the signed normal distance from the interface $d(\boldsymbol{x}, t)$.

To reconstruct the distribution of fluid properties, the actual location of the interface has to be captured. In the level-set technique fluid properties are assumed to be function of d. At $t = 0$ this function is initialized as $d > 0$ in water, $d < 0$ in air and $d = 0$ at the interface [5]. The generic fluid property f is assumed to be $f(d) = f_w$ if $d > \delta$, $f(d) = f_a$ if $d < -\delta$ and

$$f(d) = (f_w + f_a)/2 + (f_w - f_a)/2 \ \sin(\pi d/(2\delta))$$

otherwise, δ being the half width of a transition region introduced to smooth the jump in fluid properties. The same smoothing is applied to the Heaviside function H.

During the evolution the distance is transported by the flow according to the equation

$$\frac{\partial d}{\partial t} + \boldsymbol{u} \cdot \nabla d = 0 \tag{4}$$

The interface being a material surface, its location is captured as the level $d = 0$. To keep constant in time the width of the transition region the distribution of the distance function is periodically reinitialized by computing, at each cell center, the minimum distance from the interface.

Disturbances outgoing from the computational domain are damped by two beach regions located about the two ends of the domain. Let $y = 0$ to denote the still water level, eq. (4) takes the following form:

$$\frac{\partial d}{\partial t} = \boldsymbol{u} \cdot \nabla d - \nu(d + y) \tag{5}$$

where ν is zero up to the inner limits of the beaches and grows quadratically toward the boundaries of the computational domain.

The numerical solution of the Navier-Stokes equations is achieved through a finite difference solver on a non staggered grid. Cartesian velocities and pressure are defined at the cell centers while volume fluxes are defined at the mid point of the cell faces and are computed by using a quadratic upwind scheme (QUICK) to interpolate cartesian velocities. The momentum equation is integrated in time with a semi-implicit scheme: convective terms and the off-diagonal part of the diffusive ones are computed explicitly with a third-order Runge-Kutta scheme while a Crank-Nicolson discretization is employed for the diagonal part of the diffusive terms. A fractional step approach is used: an auxiliary velocity field is obtained by neglecting the pressure term on the right hand side of the momentum equation (*predictor step*) and in a second stage (*corrector step*) the velocity field is updated by adding a pressure correction contribution. The latter is obtained by enforcing continuity thus yielding to a Poisson equation which is solved by using a multigrid technique.

2.2 POTENTIAL FLOW MODEL AND COUPLING PROCEDURE

In the hydrofoil vicinities, a potential model is used which allows to describe the flow in terms of a scalar function φ. A pseudo-steady Kutta condition is applied so that the flow at the trailing edge is directed along the chord of the hydrofoil. The potential flow domain is bounded by the hydrofoil, by the ends of the computational domain at the two sides, by the bottom of the channel from below and by the matching line from the top.

Due to the incompressible assumption, the flow in the potential region is governed by the Laplace equation which solution is sought with the help of a boundary integral representation of the velocity potential. On the matching line, which is located in the water domain, the velocity potential is assigned by integrating in time the unsteady Bernoulli's equation

$$\frac{\partial \varphi}{\partial t} = -\frac{|\boldsymbol{u}|^2}{2} - gz + \frac{p^B}{\varrho_w} \tag{6}$$

where, from the continuity of the normal stresses, p^B is related to the pressure field in the free surface domain p^F through the relation

$$p^B = p^F - 2\mu_w \frac{\partial u_n}{\partial n}$$

All along the other boundaries Neumann boundary conditions are applied. The solution of the boundary integral equation provides the normal derivative of the velocity potential on the matching line and the velocity potential along the other boundaries.

The solution in the free surface domain is performed by first. This provides pressure and velocity distributions at the matching line that are used to get the source term of eq. (6). The latter is integrated in time to update the the velocity potential on the matching line which is used as Dirichlet condition for the solution of the boundary value problem. This allows to evaluate the velocity field on the matching line which is used as boundary condition for the Navier-Stokes solver at the next step.

3. NUMERICAL RESULTS

The flow about a NACA 0012 hydrofoil, 5 degrees angle of attack is simulated in the same conditions as the original experiment by Duncan [4]. The ratio between submergence and chord is 0.783. Numerical computations are carried out at a Reynolds number $Re = 1000$, significantly smaller than the experimental one, while both the Froude and Weber numbers are the same of the experiment $Fr = 0.567$ and $We = 42$. To reduce the formation of forward propagating waves generated by an impulsive start, a sinusoidal ramp is used to accelerate the hydrofoil up to the final speed which is reached at $t = 10$. Starting from these conditions, the Weber number is halved twice by varying the surface tension coefficient and three different flow regimes in the breaking zone are obtained.

In Fig. 1 and Fig. 2, the free surface profiles obtained at $t = 13.8$ and $t = 14.2$ are shown. In these pictures, differences in the breaking wave establishment

and in the air entrainment induced by the different surface tension coefficients are evident. In particular it is worth to notice the progressive suppression of the initial jet formation which is replaced by the formation of a large bulge which slides along the forward face of the wave. This process is evident in the sequence in Fig. 3 where the vorticity by density contours are shown along with the transition region.

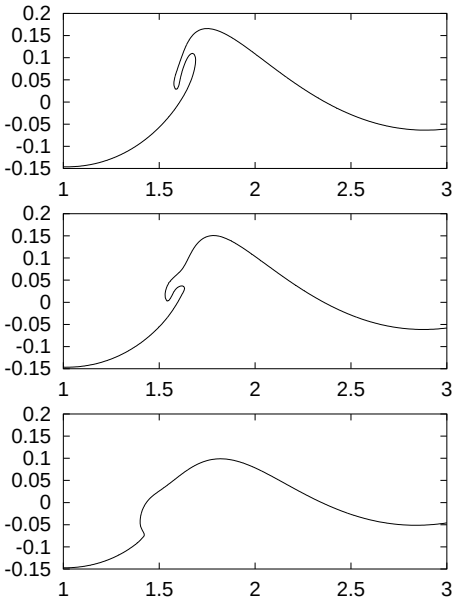

Figure 1: Different breaking onset generated by increasing value of the surface tension coefficient ($t = 14.2$). From top to bottom $We = 42, 21, 10.5$.

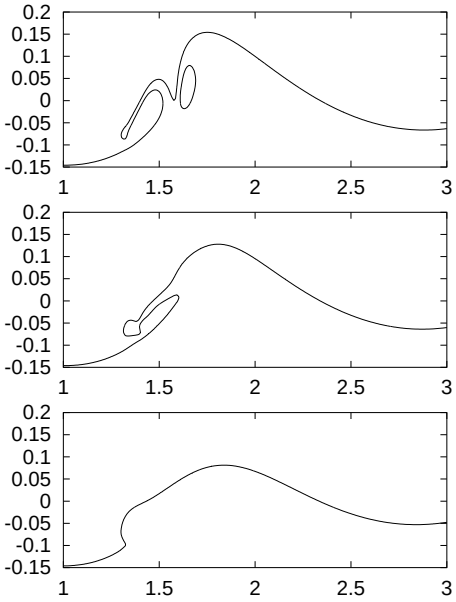

Figure 2: Effect of the surface tension coefficient onto the air-entrapment ($t = 13.8$). From top to bottom $We = 42, 21, 10.5$.

In Fig. 4 and Fig. 5 the vorticity by density contours corresponding to the configurations of Fig. 1,2 are shown. In spite of the thick transition region, a clear difference in the vorticity production mechanism appear, with the highest surface tension case characterized by a larger curvature that cause flow separation at the toe of the bulge thus resulting in a stronger vorticity production and a faster downstream diffusion.

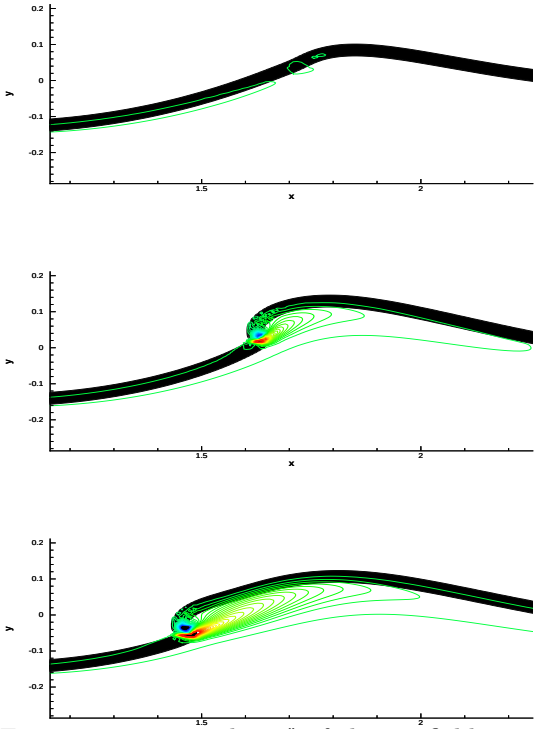

Figure 3: Time evolution of the $\omega\varrho$ field into the bulge during the breaking onset ($We = 10.5$). From top to bottom $t = 10.8, 12.8, 13.6$.

In Fig. 6 the history of the free surface profile is shown for a very long time evolution of the lowest Weber number case ($We = 10.5$). The sequence shows that the front face of the bulge slightly oscillates and downstream propagating ripples are generated each time the bulge reaches its foremost position. In the region where ripples are generated, the computational grid has a horizontal spacing $\Delta x \sim 0.01$ that means about forty grid points per ripples wavelength. As observed by Duncan [6], bulge oscillations, which slightly decay in time, are induced by the start from the rest. In the numerical results, the period of the oscillations corresponds to that measured by Duncan [6], that is about 4 times the period of the following gravity waves.

Although mechanisms responsible for the ripples formation are still under investigation, a better understanding of their propagation properties can be achieved by using the value of σ for the water, reducing the length of the body instead. In this way, the corresponding scale of the problem results in a hydrofoil length of $0.0125m$, towed at the same Fr number. With this set of values, the computation shows ripples having a dimensional wavelength of about $0.005m$, which makes their propagation highly dominated by surface tension. In fact, for $\lambda = 0.005m$, the linear theory provides a wave speed of $c \sim 1.5 c_m = 0.345 ms^{-1}$, c_m being

$0.23ms^{-1}$ for water [7], which is quite close to the ripples propagation speed $c_o \sim 0.35ms^{-1}$ recovered by numerical results.

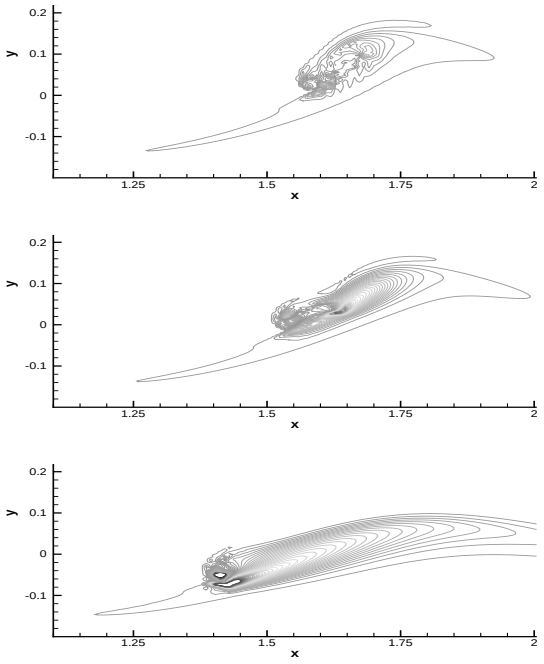

Figure 4: Contour of $\omega\varrho$ at $t = 13.8$. From top to bottom $We = 42, 21, 10.5$.

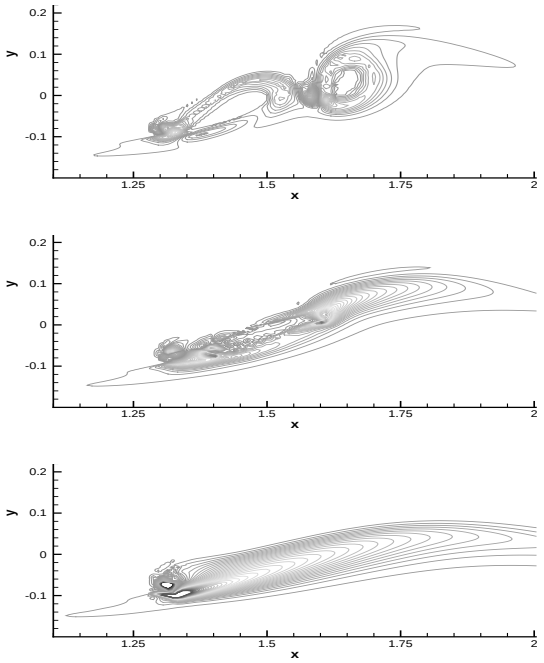

Figure 5: Contour of $\omega\varrho$ at $t = 14.2$. From top to bottom $We = 42, 21, 10.5$.

4. ACKNOWLEDGMENTS

This work has been financially supported by the *Ministero delle Infrastrutture e dei Trasporti* in the frame of the INSEAN research plan 2000-02.

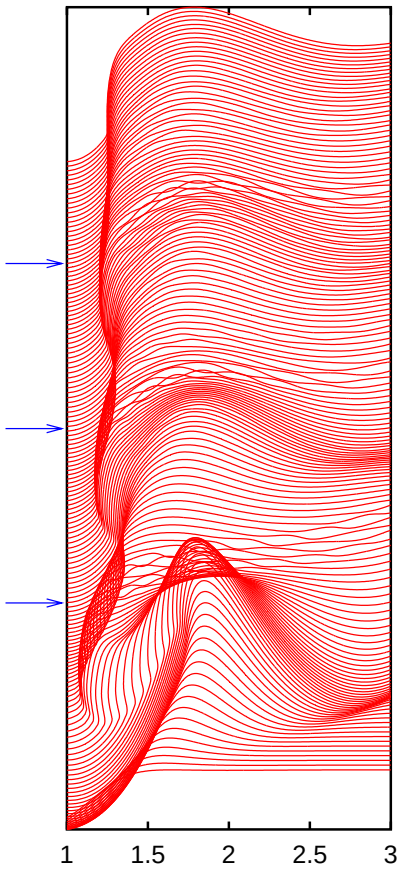

Figure 6: History of the free surface profile for the case $We = 10.5$. Arrows locate times at which downstream propagating ripples appear.

5. BIBLIOGRAPHY

1 J.U. Brackbill, D.B. Kothe and C. Zemach 'A continuum method for modeling surface tension', J. Comput. Phys., **100**, 335-354, 1992.

2 E.F. Campana, A. Iafrati 'Unsteady free surface waves by domain decomposition approach', 16^{th} IWWWFB, 9-12, 2001.

3 A. Iafrati, E.F. Campana 'A domain decomposition approach to compute breaking waves', submitted for publication on the Int. J. for Num. Meth. in Fluids, 2001.

4 J.H. Duncan, 'The breaking and non-breaking wave resistance of a two-dimensional hydrofoil', J. Fluid Mech., **126**, 507-520, 1983.

5 M. Sussman, P. Smereka and S.J. Osher 'A level-set approach for computing solutions to incompressible two-phase flow', J. Comput. Phys., **114**, 146-159, 1994.

6 J.H. Duncan, 'An experimental investigation of breaking waves produced by a towed hydrofoil', Proc. R. Soc. Lond., **A377**, 331-348, 1981.

7 J. Lighthill, 'Waves in Fluids', Cambridge Univ. Press (1978)

17th IWWWFB

Discussion Sheet

Abstract Title :	Surface tension effects of breaking waves		
(Or) Proceedings Paper No. :	06	***Page :***	021
First Author :	Campana, E.F.		
Discusser :	Yeung, R.W.		

Questions / Comments :

There is a published work either closely related or similar to your problem: Dommermuth & Mui (1995), ASME Journel of Fluids Engineering. These authors studied in detail the formation of the breaker by a very elaborate spectral solution near the toe of the breaker, with discussions on Duncan's latest experiments (see cited reference). You may be interested in some comparisons with this reference.

Author's Reply :
(If Available)

Author did not respond.